Research Square

Preprints are preliminary reports that have not undergone peer review.
They should not be considered conclusive, used to inform clinical practice,
or referenced by the media as validated information.

Sulfonated Quinoline-Malononitrile-Phenothiazine Hybrid Fluorescent Probe with D–π–A Motif: Design, Synthesis and Specific Peroxynitrite Imaging in Living Cells

Xinyu Zhao
Qingdao University of Science and Technology
Cheng Zhao
Qingdao University of Science and Technology
Taihang Meng
Qingdao University of Science and Technology
Guoyan Liu
Qingdao University of Science and Technology
Teng Mao
Qingdao University of Science and Technology
Ying Fang
Qingdao University of Science and Technology
Guorui Cao
caoguorui@qust.edu.cn

Qingdao University of Science and Technology

Research Article

Keywords: Peroxynitrite ($ONOO^-$), Fluorescent probe, Phenothiazine, Sulfonated quinoline-malononitrile, Biological imaging

Posted Date: November 19th, 2026

DOI: https://doi.org/10.21203/rs.3.rs-11452799/v1

License: This work is licensed under a Creative Commons Attribution 4.0 International License.
Read Full License

Additional Declarations: No competing interests reported.

Sulfonated Quinoline-Malononitrile-Phenothiazine Hybrid Fluorescent Probe with D–π–A Motif: Design, Synthesis and Specific Peroxynitrite Imaging in Living Cells

Xinyu Zhao[a], Cheng Zhao[b], Taihang Meng[a], Guoyan Liu[a], Teng Mao[a], Ying Fang[b], Guorui Cao[a]*

[a]State Key Laboratory of Advanced Optical Polymer and Manufacturing Technology, College of Chemical Engineering, Qingdao University of Science and Technology, Qingdao 266042, China

[b]Key Laboratory of Optic-electric Sensing and Analytical Chemistry for Life Science, MOE, College of Chemistry and Molecular Engineering, Qingdao University of Science and Technology, Qingdao, 266042, China

Corresponding author:

E-mail: caoguorui@qust.edu.cn (Guorui Cao) ORCID number: 0000-0002-2948-9298

Abstract

In this study, a novel fluorescent "turn-on" probe **M5** was designed and synthesized based on a sulfonated quinoline-malononitrile-phenothiazine hybrid system. Designed with a typical D–π–A scaffold, the probe consists of phenothiazine as the electron donor and the luminescent core, sulfonated quinoline-malononitrile (QM-SO_3) as the electron acceptor and water-solubilizing unit, and a conjugated C=C double bond as the specific recognition site for $ONOO^-$. **M5** exhibits no emission due to the strong ICT process from the phenothiazine core to the QM-SO_3 moiety, while its fluorescence is significantly activated upon $ONOO^-$-mediated cleavage of the C=C bond. **M5** possesses superior photophysical and sensing properties, including an emission maximum at 560 nm and a low detection limit of 0.30 μM. It shows high selectivity toward $ONOO^-$ with strong anti-interference capability against various biologically relevant analytes, such as reactive oxygen species (ROS), reactive nitrogen species (RNS), reactive sulfur species (RSS), and common physiological ions. Furthermore, **M5** maintains stable fluorescence emission over the physiological pH range (5–11) and exhibits good biocompatibility at concentration of 25.0 μM. Importantly, **M5** has been successfully applied for the specific fluorescent imaging of both exogenous and endogenous $ONOO^-$ in living HeLa cells. Collectively, these results confirm that **M5** is a reliable and promising tool for the accurate monitoring of $ONOO^-$ in complex biological systems, holding significant potential for investigating $ONOO^-$-related physiological and pathological processes.

Keywords: Peroxynitrite ($ONOO^-$); Fluorescent probe; Phenothiazine; Sulfonated quinoline-malononitrile; Biological imaging

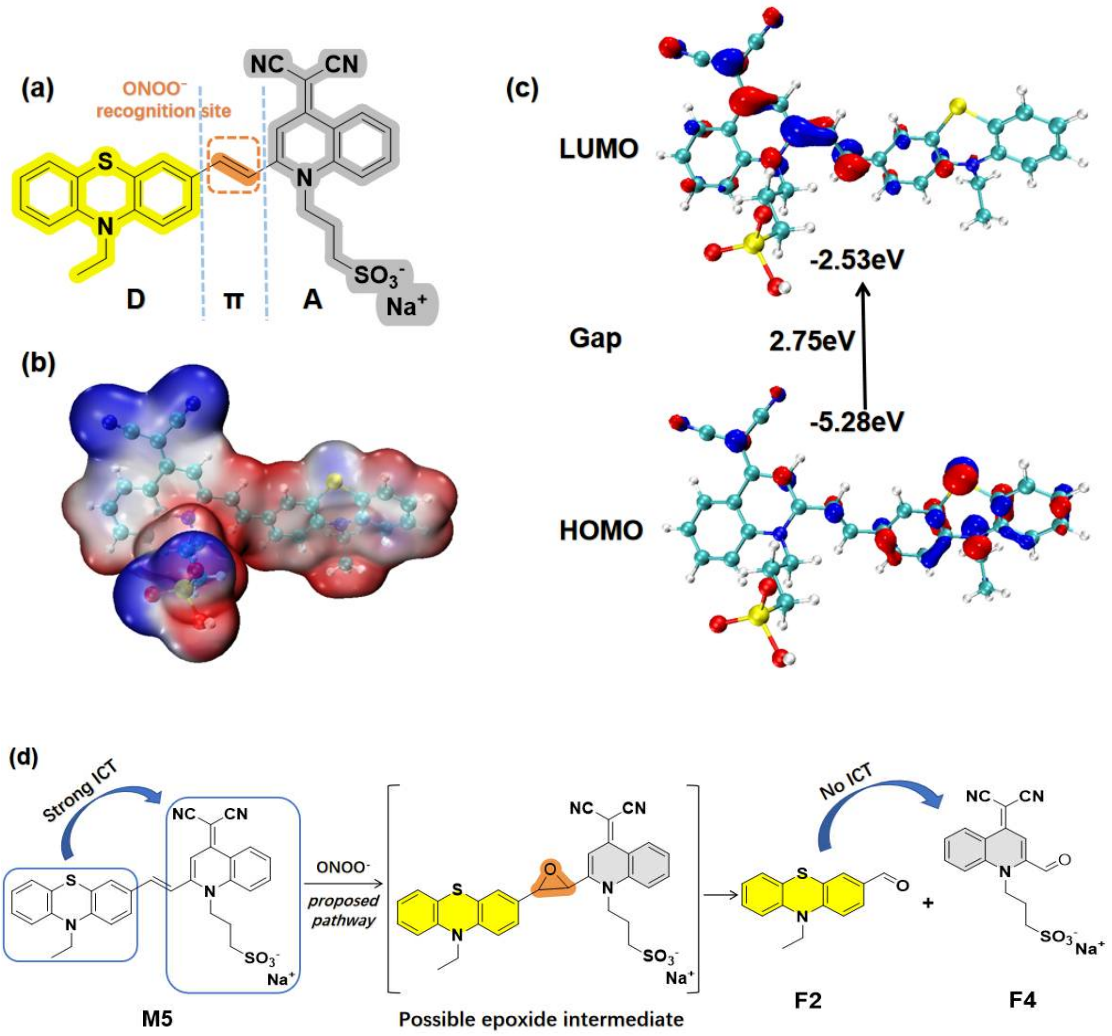
1. Introduction

Peroxynitrite ($ONOO^-$) is a type of reactive nitrogen species (RNS) that is generated by a diffusion-controlled reaction between superoxide anion and nitric oxide [1]. It plays a vital role in diverse physiological and pathological processes. Excessive accumulation of this species in living organisms can induce oxidative and nitrative modifications of biological macromolecules. $ONOO^-$ is closely associated with the pathogenesis and progression of malignant tumors [2], diabetes, cardio-cerebrovascular diseases, some inflammatory illnesses [3,4], and neurodegenerative diseases [5] such as Alzheimer's disease [6]. Thus, accurate detection of $ONOO^-$ is essential for exploring its biological functions and disease mechanisms [7].

Recently, in order to achieve the detection of peroxynitrite, many methods have been developed including electrochemical analysis [8], electron spin resonance [9], and ultraviolet-visible spectrophotometry [10]. Nevertheless, these methods still suffer from several drawbacks, including unsatisfactory detection selectivity, the lack of capacity for in situ detection, and insufficient sensitivity [11]. Fluorescence imaging has attracted widespread attention in the field of biological analysis with high sensitivity, high spatiotemporal resolution, high efficiency and minimal invasiveness [12,13]. However, fluorescent probes still face several challenges, such as poor photostability, limited capability to modulate the intramolecular charge transfer (ICT) effect and poor selectivity [14–16].

In this work, we decorate a quinoline-malononitrile (QM) moiety with a phenothiazine core to prepare a novel fluorescent probe **M5** for $ONOO^-$ detection (Scheme 1a). In this probe, QM possesses superior photophysical properties, favorable biocompatibility, and facile structural derivatization. Zhu et al. [17]

modified QM with sulfonate groups to improve its water solubility. In this structure, the sulfonic acid-modified QM acts as an electron acceptor, the C=C double bond serves as the recognition unit, and the phenothiazine acts as the fluorophore and electron donor. Phenothiazine is widely recognized as an electron-rich donor moiety owing to the presence of nitrogen and sulfur atoms in its heterocyclic framework. Furthermore, structural modification at the nitrogen position can influence the electronic structure and photophysical properties of phenothiazine-based donor–acceptor systems, providing opportunities for tuning their intramolecular charge transfer (ICT) characteristics [18–20]. The sulfur and nitrogen atoms in the heterocycle have strong electron-donating abilities, facilitating efficient regulation of ICT [21]. Conjugated C=C bonds can be selectively oxidatively cleaved by $ONOO^-$ [22]. The negligible fluorescence of the intact probe may be attributed to the strong donor–acceptor interaction and the associated intramolecular charge-transfer character, which provides an efficient nonradiative relaxation pathway. In recent years, various fluorescent probes with different molecular scaffolds and recognition strategies have been developed for the selective detection and fluorescence imaging of $ONOO^-$ in biological systems [23–27]. This probe generates a highly sensitive fluorescent signal in response to $ONOO^-$, together with excellent selectivity, favorable biocompatibility, and a low limit of detection. Moreover, it achieves distinct fluorescence imaging of both exogenous and endogenous $ONOO^-$ at the cellular level. Owing to these outstanding sensing characteristics, probe M5 holds great potential for applications and offers a new and efficient strategy for the detection of $ONOO^-$ in complex biological microenvironments.



Scheme 1. (a) Design strategy and chemical structure of **M5.** (b) Electrostatic potential distribution on the surface of **M5**. (c) Frontier molecular orbital profiles of **M5** based on DFT (B3LYP/6-31G*) calculations. (d) The proposed sensing mechanism of **M5** toward $ONOO^-$.

2. Experimental section

2.1 Reagents and apparatus

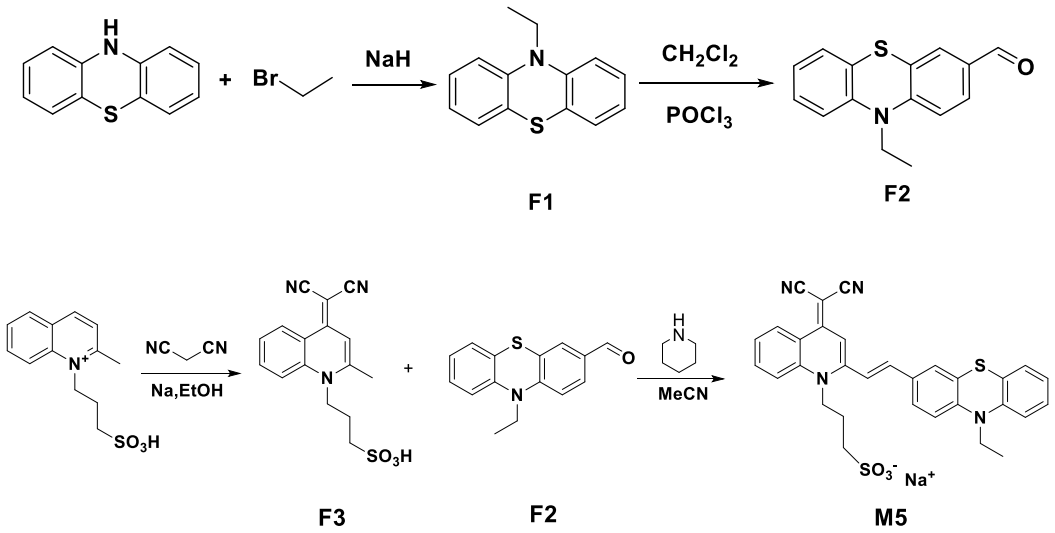
Unless otherwise stated, all reagents were purchased from commercial suppliers and used without further purification. Solvents used were purified by standard methods prior to use. Twice-distilled water was used throughout all experiments. HRMS mass spectra were measured on a Waters ACQUITY UPLC H-Class. ^1H NMR and ^{13}C

NMR spectra were measured on a Bruker DMX 500 spectrometer. Absorption spectra were measured on a SHIMADZU UV-2600i spectrophotometer. Fluorescence emission spectra were obtained using a SHIMADZU RF-6000 spectrofluorometer. The pH measurements were carried out on a Mettler-Toledo Delta 320 pH meter.

HPLC analysis was performed on an Agilent 1220 Infinity II system equipped with an Agilent HC-C18(2) column (250 × 4.6 mm, 5 μm). The mobile phase consisted of acetonitrile (A) and water (B) (v/v). The gradient elution program was as follows: 0–10 min, 50→90% A; 10–15 min, 90% A; 15–15.01 min, 90→50% A; 15.01–20 min, 50% A. The flow rate was 0.8 mL/min, the detection wavelength was 254 nm, the column temperature was 25 °C, and the injection volume was 5 μL.

2.2 Synthesis of compounds

The synthetic route of probe **M5** is shown in Scheme 2, with key steps as follows: Using 10H-phenothiazine as the starting material, we obtained 10-ethylphenothiazine (F1) via *N*-ethylation to modify the electron-donating fluorophore. F1 was formylated through the Vilsmeier–Haack reaction to synthesize 10-ethylphenothiazine-3-carbaldehyde (F2), providing the aldehyde group required for subsequent condensation reactions. 3-(2-methylquinolin-1-yl)propane-1-sulfonic acid inner salt reacted with malononitrile catalyzed by sodium ethoxide to generate intermediate F3 containing quinoline sulfonic acid group. Under a nitrogen atmosphere, F2 and F3 were refluxed in acetonitrile at 90 °C for 8 h with piperidine as the catalyst to obtain the target probe **M5**. The structure of **M5** was confirmed by ^{1}H NMR, ^{13}C NMR and HRMS (Figures S12–S14).



Scheme 2. Synthetic routes of M5

2.3 Synthesis of F1

Sodium hydride (2.40 g, 60.0 mmol, 60% suspension in mineral oil) was added to a solution of 10H-phenothiazine (8.00 g, 40.1 mmol) in 100.0 mL dry DMF under a nitrogen atmosphere. After the mixture had been stirred in an ice bath for 30.0 min, a solution of bromoethane (5.60 g, 51.4 mmol) in 33.0 mL dry DMF was added dropwise to the reaction mixture. The mixture was then allowed to warm to room temperature and stirred for 12 h. After the reaction was complete, saturated aqueous NaCl solution was added and the product was extracted with ethyl acetate (3 × 100.0 mL). The combined organic layers were dried over Na_2SO_4, filtered to remove solids, and the filtrate was concentrated under reduced pressure. The crude product was purified by column chromatography to yield the product F1 as a white solid (8.70 g, 95% yield) [28]. Melting point: 89–90 °C. Fourier-transform infrared (FT-IR) spectroscopy: 3442, 3053, 2982, 2932, 2861, 1902, 1791, 1627, 1590, 1440 cm^{-1}; ^1H NMR (500 MHz, DMSO-d_6): δ 7.20–7.17 (m, 2H), 7.14 (dd, J_1 = 7.5 Hz, J_2 = 1.5 Hz, 2H), 7.01 (dd, J_1 = 8.5 Hz, J_2 = 1.5 Hz, 2H), 6.95–6.92 (m, 2H), 3.91 (q, J_1 = J_2 = 5.0 Hz, 2H), 1.29 (t, J = 5.0 Hz, 3H); ^{13}C NMR (125 MHz, DMSO-d_6): δ 144.9, 128.1,

127.5, 123.5, 122.8, 115.9, 41.5, 13.2; HRMS (ESI^+) m/z: calcd for $C_{14}H_{13}NS$ $[M+Na]^+$ 250.0666, found 250.0656.

2.4 Synthesis of F2

$POCl_3$ (3.0 mL) was mixed with DMF (3.0 mL) in an ice bath for 1 h to prepare the Vilsmeier–Haack reagent. A solution of 10-ethylphenothiazine (4.50 g, 19.8 mmol) in anhydrous dichloromethane (15.0 mL) was then added dropwise. The reaction mixture was transferred to a pressure-resistant reaction tube, sealed, and heated in an oil bath maintained at 75 °C overnight. After cooling to room temperature, the reaction mixture was carefully poured into ice water (100.0 mL) and extracted with dichloromethane (3 × 50.0 mL). After the organic solvent was removed under reduced pressure, F2 was purified by column chromatography to give a yellow solid (4.01 g, 80% yield) [29]. Melting point: 93–95 °C. Fourier-transform infrared (FT-IR) spectroscopy: 3446, 2930, 2827, 2738, 1552, 1441, 1339, 1199, 1102, 1042 cm^{-1}; ^1H NMR (500 MHz, $CDCl_3$): δ 9.78 (s, 1H), 7.62 (dd, J_1 = 5 Hz, J_2 = 10 Hz, 1H), 7.56 (d, J = 2.0 Hz, 1H), 7.17–7.14 (m, 1H), 7.10–7.08 (m, 1H), 6.97–6.94 (m, 1H), 6.90–6.88 (m, 2H), 3.97 (q, J_1 = J_2 = 5.0 Hz, 2H), 1.44 (t, J = 5.0 Hz, 3H); ^{13}C NMR (125 MHz, $CDCl_3$): δ 188.9, 149.2, 142.0, 129.9, 129.2, 127.1, 126.6, 126.4, 123.4, 122.5, 122.1, 114.5, 113.3, 41.4, 11.8; HRMS (ESI^+) m/z: calcd for $C_{15}H_{13}NOS$ $[M+H]^+$ 256.0796, found 256.0792.

2.5 Synthesis of F3

3-(2-Methylquinolin-1-ium-1-yl)propane-1-sulfonate (5.00 g, 19.0 mmol) and malononitrile (1.24 g, 18.8 mmol) were dissolved in ethanol (40.0 mL). The mixture was stirred in an ice bath, and a solution of sodium (0.45 g) in dry ethanol (20.0 mL) was added. After the addition, the reaction mixture was stirred at room temperature overnight. Dilute hydrochloric acid (1 M) was added to adjust the pH to 3–4. The

resulting mixture was concentrated to dryness under reduced pressure, and the residue was purified by column chromatography to afford F3 as a yellow solid (2.50 g, 40% yield) [30]. Melting point: 245–247 °C. Fourier-transform infrared (FT-IR) spectroscopy: 3442, 2927, 2196, 1601, 1553, 1473, 1437, 1381, 1346, 1048 cm^{-1}; ^{1}H NMR (500 MHz, DMSO-d_6): δ 8.93 (dd, J_1 = 8.5 Hz, J_2 = 1.5 Hz, 1H), 8.26 (d, J = 10.0 Hz, 1H), 7.92–7.88 (m, 1H), 7.62–7.58 (m, 1H), 6.82 (s, 1H), 4.60 (t, J = 10.0 Hz, 2H), 2.68 (s, 3H), 2.64 (t, J = 5.0 Hz, 2H), 2.03–1.99 (m, 2H); ^{13}C NMR (125 MHz, DMSO-d_6): δ 152.5, 150.9, 138.2, 133.5, 125.0, 124.8, 120.7, 120.5, 119.3, 118.3, 109.1, 47.7, 47.1, 45.8, 24.2, 21.3; HRMS (ESI^-) m/z: calcd for $C_{16}H_{15}N_3O_3S$ $[M-H]^-$ 328.0761, found 328.0760.

2.6 Synthesis of M5

Under a nitrogen atmosphere, F2 (0.41 g, 1.6 mmol) and F3 (0.53 g, 1.6 mmol) were refluxed in acetonitrile (8.0 mL) at 90 °C for 8 h with piperidine (0.48 g, 5.63 mmol). Afterward, the solvent was removed under reduced pressure. The residue was poured into water and extracted with dichloromethane. The organic extracts were washed with saturated $NaHCO_3$ solution, concentrated, and purified by column chromatography to afford **M5** as an orange solid (0.12 g, 13% yield). Melting point: 180–199 °C. Fourier-transform infrared (FT-IR) spectroscopy: 3437, 2932, 2855, 2192, 1586, 1544, 1500, 1466, 1430, 1359 cm^{-1}; ^{1}H NMR (500 MHz, DMSO-d_6): δ 8.92 (d, J = 5.0 Hz, 1H), 8.24 (d, J = 10.0 Hz, 1H), 7.90 (t, J = 5.0 Hz, 1H), 7.75–7.73 (m, 2H), 7.61–7.58 (m, 2H), 7.36 (d, J = 15.0 Hz, 1H), 7.21 (t, J = 15.0 Hz, 1H), 7.15 (d, J = 10.0 Hz, 1H), 7.07 (s, 1H), 7.03 (t, J = 10.0 Hz, 2H), 6.96 (t, J = 5.0 Hz, 1H), 4.74 (t, J = 10.0 Hz, 2H), 3.97 (q, J_1 = J_2 = 5.0 Hz, 2H), 2.69 (t, J = 5.0 Hz, 2H), 2.12

(s, 2H), 1.33 (t, J = 5.0 Hz, 3H); ^{13}C NMR (125 MHz, DMSO-d_6): δ 152.5, 149.9, 145.9, 143.8, 139.5, 138.5, 134.2, 130.0, 129.1, 128.3, 127.5, 127.0, 125.4, 125.4, 123.4, 123.3, 122.5, 121.0, 118.8, 118.7, 116.0, 115.6, 106.8, 49.1, 48.0, 46.6, 41.9, 24.8, 12.9; HRMS (ESI$^-$) m/z: calcd for $C_{31}H_{25}N_4NaO_3S_2$ [M-Na]$^-$ 565.1374, found 565.1372.

2.7 Optical measurements

For photophysical measurements, compound **M5** was dissolved in DMSO to prepare a 1 mM stock solution. The stock solution was further diluted to a final concentration of 10.0 μM with DMSO/H_2O (8:2, v/v) for subsequent spectroscopic tests.

Sources for different ROS/RNS are described as follows. Specifically, H_2O_2 and TBHP solutions were purchased from Sigma-Aldrich and added to the probe solution directly. The source of NaOCl was commercial bleach. Hydroxyl radical (•OH) and t-BuOO• were generated by the Fenton reaction. Briefly, ferrous chloride ($FeCl_2$) was added in the presence of 10 equiv. of H_2O_2 and TBHP. The concentration of •OH was equal to the Fe(II) concentration. Peroxynitrite ($ONOO^-$) solution was synthesized according to a reported procedure. Briefly, a mixture of sodium nitrite (0.6 M) and hydrogen peroxide (0.7 M) was acidified with hydrochloric acid (0.6 M), and sodium hydroxide (1.5 M) was added within 1–2 seconds to make the solution alkaline. The excess hydrogen peroxide was removed by passing the solution through a short column of manganese dioxide. The concentration of peroxynitrite was determined by measuring the absorption of the solution at 302 nm. The extinction coefficient of peroxynitrite solution in 0.1 M NaOH is 1,670 M^{-1} cm^{-1} at 302 nm. The rest of the interfering ions come from the corresponding salt solutions.

2.8 Cell cytotoxicity test

HeLa cells (1.0×10^4 cells/well) were incubated in culture media in 96-well plates at 37 °C in a 5% CO_2 incubator for 24 h, and then different concentrations of **M5** (0, 10, 20, 30, 40, 50, 60, 70, 80, 90, 100 μg/mL) were added to the wells and the cells were incubated for another 24 h. 15 μL of MTT solution (5 mg/mL in phosphate buffer solution) was added to each well. Then, the plate was incubated in the 5% CO_2 incubator for an additional 4 h; the absorbance values of the wells were recorded using a microplate reader at 490 nm. Cell viability (%) was calculated by the following equation: Cell viability (%) = $A/A_0 \times 100\%$. Here, A and A_0 are the absorbances of the experimental group and the control group, respectively. Each concentration was tested in triplicate across three independent experiments, with cytotoxicity assessed using the MTT assay.

2.9 Cell culture and imaging

Cell culture. All cells were cultured in Dulbecco's Modified Eagle's Medium (DMEM) supplemented with 10% fetal bovine serum (FBS) and 1% antibiotics (100 U/mL penicillin and 100 μg/mL streptomycin) at 37 °C in a humidified atmosphere of 5% CO_2 for 24 h.

All experiments were conducted in live cells. The living-cell imaging was performed on a Nikon Ti2U microscope at 20× magnification. **M5** was excited at 405 nm, and the emission was collected in the range of 520–580 nm.

3. Results and discussion

3.1 Design and synthesis of probe M5

Based on the strong oxidizing property of peroxynitrite ($ONOO^-$), we designed a novel donor–π–acceptor (D–π–A) type probe, **M5**. The molecular scaffold integrates a phenothiazine donor and a sulfonated quinoline-malononitrile (QM-SO_3) acceptor

linked via a C=C π-bridge [31–34]. The QM-SO_3 endows the probe with favorable water solubility and excellent biocompatibility [35,36]. The phenothiazine moiety provides stable photophysical properties, controllable ICT, favorable electron-donating capacity, and pH tolerance. The strong oxidizing and nucleophilic properties of $ONOO^-$ can trigger the specific oxidative cleavage of the C=C double bond. **M5** exhibited weak fluorescence due to the strong ICT process from the phenothiazine core to the QM-SO_3 moiety [37,38], which could facilitate nonradiative relaxation of the excited state. While treating with $ONOO^-$, cleavage of the C=C bridge disrupts the D–π–A conjugated system, thus weakening the ICT process and arousing a bright yellow emission (Scheme 1d) [39–41]. This enables the selective detection of $ONOO^-$ in complex biological systems.

To rationalize the molecular structure and electronic properties of **M5**, DFT calculations were performed to optimize its ground-state geometry at the B3LYP/6-31G(d) level in a DMSO solvent field using Gaussian 09. As shown in Scheme 1c, the highest occupied molecular orbital (HOMO) of **M5** is mainly distributed over the phenothiazine donor, with an energy of −5.28 eV, while the lowest unoccupied molecular orbital (LUMO) is mainly localized on the quinoline-malononitrile (QM-SO_3) acceptor, with an energy of −2.53 eV. Notably, the HOMO and LUMO exhibit nearly complete spatial separation, with minimal orbital overlap, indicating a pronounced electronic distinction between the donor and acceptor units. The spatial separation of the HOMO and LUMO suggests possible photoinduced electron-density redistribution from phenothiazine to QM-SO_3 in the excited state, demonstrating clear intramolecular charge transfer (ICT) characteristics. Analysis of the molecular electrostatic potential (MEP) provides insight into the charge distribution across different regions of the molecule (Scheme 1b). The MEP

map shows a negative potential region over the phenothiazine moiety (red region) and a positive potential region over the QM-SO_3 unit (blue region). Collectively, these computational results provide theoretical support for the D–π–A electronic structure and the proposed ICT characteristics of **M5**.

3.2 Spectral responses of M5 to $ONOO^-$

The photophysical properties of probe **M5** were first systematically investigated by determining its UV-vis absorption and fluorescence emission spectra before and after reaction with peroxynitrite ($ONOO^-$). The results showed that **M5** exhibited no fluorescence before the reaction and had an absorption maximum at 449 nm. After the reaction, a new emission maximum appeared at 560 nm (Figure 1). After reacting with $ONOO^-$, the maximum UV absorption wavelength undergoes a blue shift, and the fluorescence intensity is significantly enhanced. Meanwhile, the color of the solution changes from orange-yellow to soft yellow, the characteristic absorption peak at 449 nm disappears completely, and the fluorescence emission at 560 nm is significantly activated. Benefiting from the turn-on response of **M5**, the recognition of the target analyte by this probe is characterized by a distinct signal transition—no fluorescence before the reaction and a sharp increase in fluorescence intensity after the reaction—instead of the emission wavelength shift observed with traditional probes. Therefore, it can minimize potential detection errors caused by signal crosstalk.

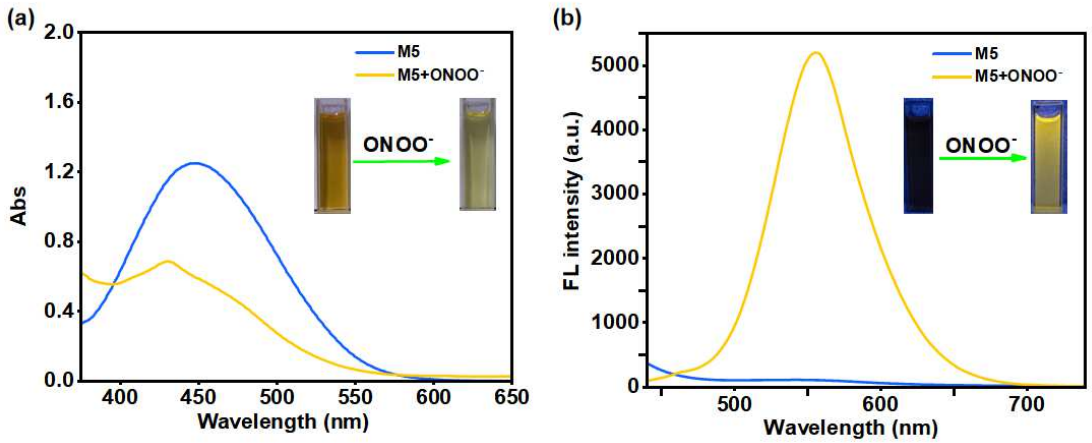


Figure 1. (a) UV-vis absorption spectra of **M5** (10.0 μM) in the absence and presence of $ONOO^-$ (0.3 mM) in DMSO/H_2O (8:2, v/v); wavelength range: 200–800 nm; temperature: 25 °C. Inset: Photograph of the solution under ambient light, showing a color change from orange to translucent yellow upon addition of $ONOO^-$. (b) Fluorescence spectra of **M5** (10.0 μM) in the absence and presence of $ONOO^-$ (0.3 mM) in DMSO/H_2O (8:2, v/v); wavelength range: 405–810 nm; λ_{ex} = 405 nm; excitation/emission slit widths: 5 nm; temperature: 25 °C. Inset: Photograph of the solution under a 365 nm UV lamp, showing a color change from brown to bright yellow upon addition of $ONOO^-$.

3.3 Optical stability evaluation and specific selectivity of M5 toward $ONOO^-$

The carbon-carbon double bond serves as a common recognition site for both nucleophilic and oxidizing species, inherently rendering the probe susceptible to interference from various potential substances. To systematically evaluate the selectivity of **M5**, it was subjected to interaction tests with a panel of biologically relevant metabolites, including reactive oxygen species (ROS: t-BuOO•, •OH, H_2O_2, HClO, $^1O_2$, TBHP), reactive nitrogen species (RNS: NO, NO_2^-), reactive sulfur species (RSS: SO_3^{2-}, S^{2-}, $S_2O_3^{2-}$, SCN^-, Cys, Hcy, GSH, etc.), and common physiological ions (CO_3^{2-}, Zn^{2+}, Al^{3+}, Ca^{2+}, K^+, Na^+, Fe^{2+}, Fe^{3+}, Mg^{2+}, etc.). As

illustrated in Figure 2a, none of these interfering substances triggered a fluorescence "turn-on" effect with an excitation wavelength of 405 nm. The selectivity of **M5** was also evaluated through competitive experiments (Figure 2b). In the presence of various relevant interfering species **M5** still exhibited a remarkable fluorescence turn-on response to $ONOO^-$. As shown in Figure 2b, the interfering species alone caused negligible fluorescence changes, whereas the subsequent addition of $ONOO^-$ led to a dramatic enhancement in fluorescence intensity, demonstrating the excellent selectivity and anti-interference capability of **M5** toward $ONOO^-$, thus laying a solid foundation for its reliable application in complex physiological microenvironments.

The fluorescence response kinetics of M5 toward $ONOO^-$ were investigated by monitoring the time-dependent changes in fluorescence intensity at 560 nm. As shown in Figure S16, the fluorescence intensity began to increase noticeably after approximately 20 min and reached a plateau at around 60 min, indicating a time-dependent response to $ONOO^-$ under the experimental conditions. Furthermore, the fluorescence intensity remained relatively stable during the subsequent observation period (60–90 min). These results provide information on the response kinetics and fluorescence signal stability of M5 under the tested conditions.

Physiological pH fluctuations may directly affect the response performance and stability of fluorescent probes. Therefore, the intrinsic fluorescence stability of **M5** and its response efficacy toward $ONOO^-$ were systematically evaluated across the physiologically relevant pH range of 5–11. As shown in Figure S17, M5 exhibited weak background fluorescence over the investigated pH range, whereas the fluorescence intensity increased significantly upon addition of $ONOO^-$ and remained relatively stable between pH 5 and 11. These results further verify **M5**'s favorable adaptability to physiological environments. Under optimized experimental conditions,

fluorescence titration experiments were conducted to systematically evaluate the quantitative detection capability of **M5** for $ONOO^-$ (Figure 3). With the gradual increase of $ONOO^-$ concentration, the fluorescence emission at 560 nm exhibited a distinct concentration-dependent enhancement, which was well fitted to the linear equation y = 499.2378 + 15.98629x (R^2 = 0.99634), with a low detection limit of 0.30 μM. When the $ONOO^-$ concentration exceeded 270 μM, the fluorescence response approached saturation, and the linear relationship was no longer maintained. Collectively, the above characterization results confirmed that **M5** integrates the core advantages of high specificity, favorable stability, and high sensitivity, and holds broad application prospects in the field of accurate quantitative detection of $ONOO^-$ in biological systems.

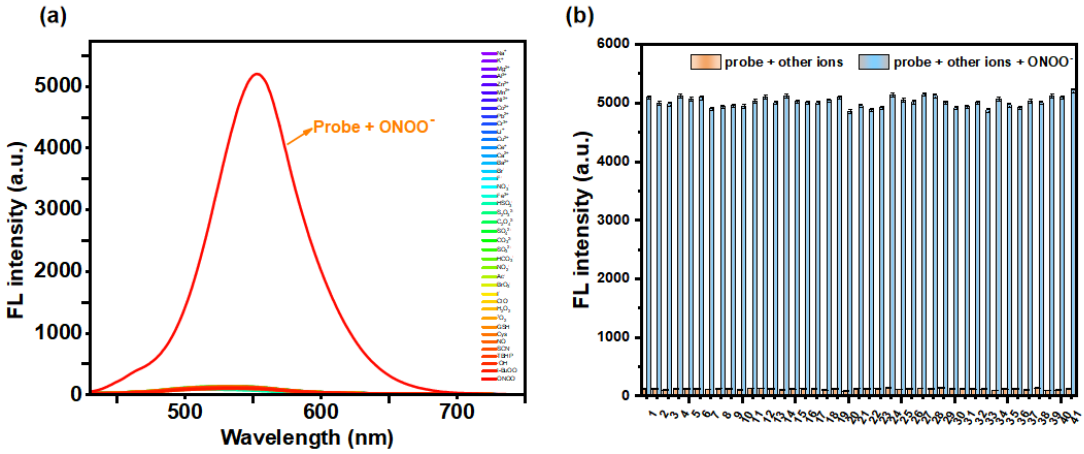


Figure 2. (a) Fluorescence responses of **M5** (10.0 μM) in DMSO/H_2O (8:2, v/v) to $ONOO^-$ (0.3 mM) and other analytes (0.3 mM), wavelength range: 405–810 nm; λ_{ex} = 405 nm, λ_{em} = 560 nm; excitation/emission slit widths: 5 nm; temperature: 25 °C. (b) Fluorescence responses of **M5** (10.0 μM) to $ONOO^-$ (0.3 mM) in the presence of other analytes (0.3 mM) in DMSO/H_2O (8:2, v/v), orange bars: **M5** + other analytes; blue bars: **M5** + other analytes + $ONOO^-$, (in the following order: 1, Na^+; 2, K^+; 3, Mg^{2+}; 4, Al^{3+}; 5, Zn^{2+}; 6, Mn^{2+}; 7, Ni^{2+}; 8, Co^{2+}; 9, Pb^{2+}; 10, Cr^{3+}; 11, Li^+; 12, Cu^{2+}; 13,

Ce^{+}; 14, Ca^{2+}; 15, Ba^{2+}; 16, Br^{-}; 17, F^{-}; 18, NO_3^{-}; 19, Fe^{3+}; 20, HSO_3^{-}; 21, $S_2O_3^{2-}$; 22, $C_2O_4^{2-}$; 23, SO_4^{2-}; 24, CO_3^{2-}; 25, SO_3^{2-}; 26, HCO_3^{-}; 27, NO_2^{-}; 28, Ac^{-}; 29, BrO_3^{-}; 30, I^{-}; 31, ClO^{-}; 32, H_2O_2; 33, $^1O_2$; 34, GSH; 35, Cys; 36, NO; 37, SCN^{-}; 38, TBHP; 39, •OH; 40, t-BuOO•; 41, blank).

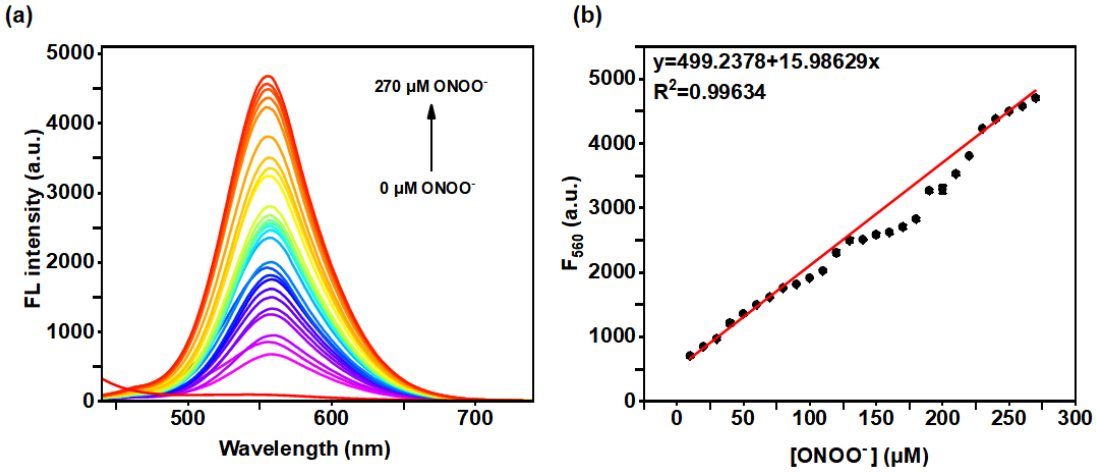


Figure 3. (a) Fluorescence spectra of **M5** (10.0 μM) upon addition of increasing concentrations of $ONOO^{-}$ (0–270.0 μM) in DMSO/H_2O (8:2, v/v), wavelength range: 405–810 nm; λ_{ex} = 405 nm, λ_{em} = 560 nm; excitation/emission slit widths: 5 nm; temperature: 25 °C. (b) The linear relationship of emission intensities at 560 nm to $ONOO^{-}$ (10.0–270.0 μM).

3.4 Response mechanism

Based on the nucleophilicity and oxidizing ability of $ONOO^{-}$, combined with previous literature reports [42–45], we hypothesized that $ONOO^{-}$ could cleave the carbon–carbon double bond of **M5**, releasing F2 and F4. As illustrated in Scheme 1d, the reaction of **M5** with $ONOO^{-}$ is proposed to proceed via a possible epoxide intermediate. $ONOO^{-}$ first attacks the C=C bond of **M5** to form the possible epoxide intermediate, which then undergoes C–C bond cleavage to afford F2 and F4. To verify this proposed pathway, the reaction mixture was subjected to HRMS analysis. As shown in Figure S19, an HRMS signal at m/z 581.1326 (ESI^{-}, calcd for

$C_{31}H_{25}N_4NaO_4S_2$ [M−Na]$^-$: 581.1323) was detected, consistent with the formation of a monooxygenated M5 species, which was tentatively assigned to a possible epoxide intermediate. Due to its instability, the intermediate could not be isolated and was only tentatively identified by HRMS. In addition, as shown in Figure 4, two key peaks corresponding to F2 (HRMS (ESI$^+$) m/z: calcd for $C_{15}H_{13}NOS$ [M+H]$^+$ 256.0796, found 256.0792) and F4 (HRMS (ESI$^-$) m/z: calcd for $C_{16}H_{12}N_3NaO_4S$ [M-Na]$^-$ 342.0554, found 342.0556) were detected. These two mass peaks in the reaction mixture are consistent with those of F2 and F4. This result supports the mechanism that **M5** reacts with $ONOO^-$ via possible epoxide formation followed by C–C bond cleavage to generate F2 and F4. To further confirm our hypothesis, we conducted HPLC analysis of the standard compounds F2, F3, and **M5** to compare their retention times with those of the reaction mixture after the reaction of **M5** with $ONOO^-$. The analysis of the chromatographic results (Figures 6a–d) was as follows: under the established HPLC conditions, the retention times of reactants F2 and F3 (Figures 6a and 6b) were approximately 15.2 min and 2.3 min, respectively. After purification of the reaction mixture, the target product **M5** (Figure 6c) exhibited a major chromatographic peak at approximately 3.5 min, and no chromatographic peaks corresponding to F2, F3, or other impurities were detected. In the chromatogram of the reaction mixture of **M5** with $ONOO^-$ (Figure 6d), the retention time of 15.2 min was basically consistent with that obtained from the single-standard injection of F2. Meanwhile, a new peak appeared with a retention time of 6.5 min, which was presumed to be product F4 generated during the reaction. This comprehensive series of experiments further demonstrated the reaction outcome.

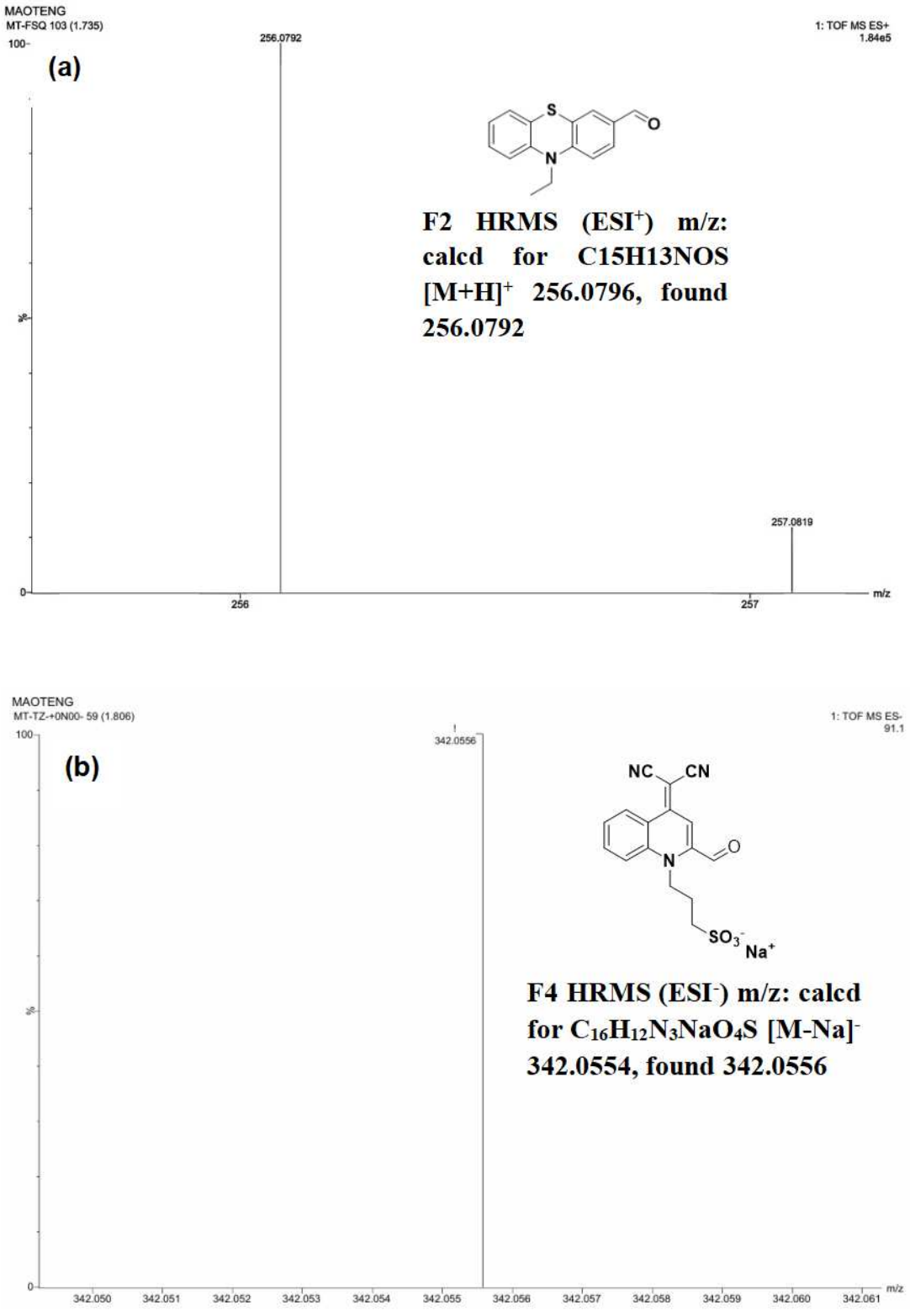


Figure 4. HRMS spectra of **F2** (a) and **F4** (b).

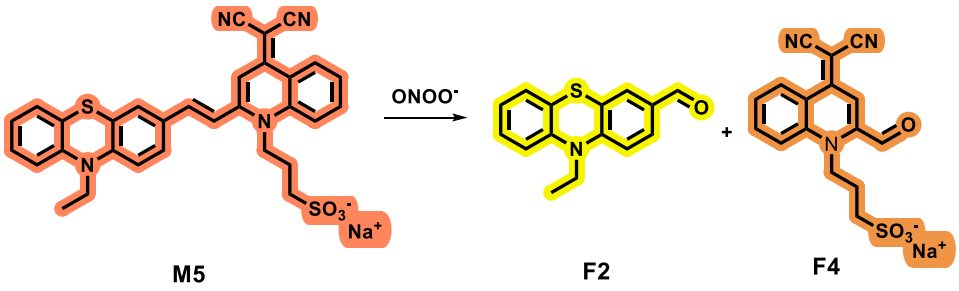


Figure 5. Proposed reaction mechanism of **M5** with $ONOO^-$.

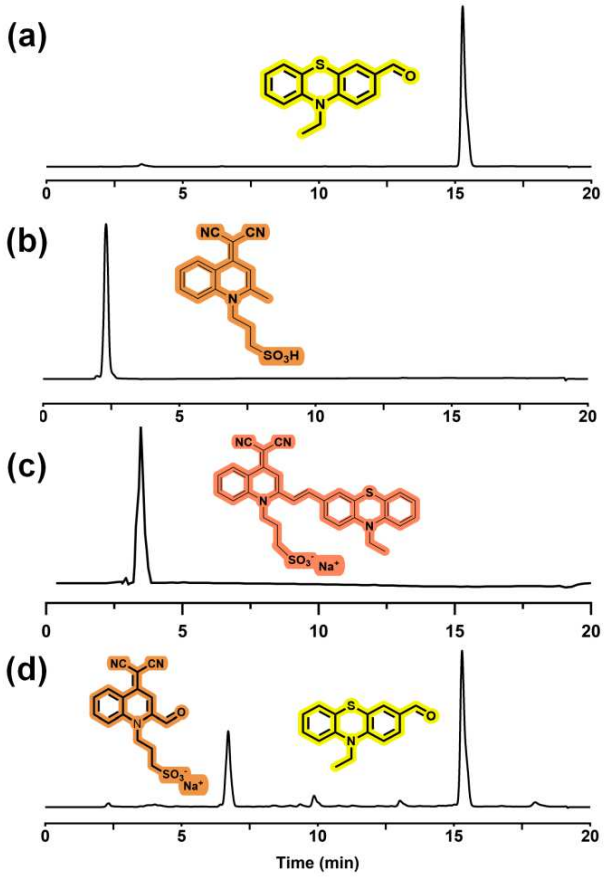


Figure 6. HPLC chromatograms of probe **M5**, its intermediates, and the reaction mixture before and after reaction with $ONOO^-$.

3.5 Fluorescence imaging of M5 in living cells

Inspired by the excellent in vitro experimental results described above, we further systematically evaluated the specific detection performance of probe **M5** for $ONOO^-$ in living cells. The results of the MTT cytotoxicity assay demonstrated that the cell viability remained at a high level at the concentration of 25.0 μM (Figure S18),

confirming that **M5** possesses favorable biocompatibility for bioimaging applications and thus laying a solid foundation for subsequent cellular experiments.

After HeLa cells were incubated with **M5**, the cells exhibited a non-fluorescent state, and no specific signal was detected in the green channel. This observation indicated that the probe maintains good structural stability in the complex intracellular microenvironment without undergoing non-specific activation (Figure 7a–c). In contrast, when the cells were stimulated with 3-morpholinosydnonimine hydrochloride (SIN-1), an exogenous $ONOO^-$ donor, the fluorescence signal in the green channel was significantly enhanced. This phenomenon was attributed to the specific interaction between **M5** and $ONOO^-$ generated by the decomposition of SIN-1 in the cells, which triggered the fluorescence "turn-on" response of the probe (Figure 7d–f). To further verify the specificity of the fluorescence response, the cells were pretreated with uric acid (UA), an $ONOO^-$ scavenger. Consequently, the aforementioned fluorescence enhancement effect was effectively suppressed, characterized by the complete disappearance of the signal in the green channel and the recovery of the cells to the non-fluorescent background state (Figure 7g–i). This clearly confirmed that the fluorescence signal was derived from the specific reaction between **M5** and $ONOO^-$ rather than the interference from other reactive species.

For the detection of endogenous $ONOO^-$ (Figure 8), the cells were co-stimulated with lipopolysaccharide (LPS) and interferon-γ (IFN-γ) to induce the production of endogenous $ONOO^-$. The results showed that the fluorescence variation trend was consistent with that of the exogenous $ONOO^-$ stimulation group, indicating that **M5** can efficiently capture endogenously generated $ONOO^-$ in cells. In summary, the above experimental results fully confirmed that **M5** is a reliable specific fluorescent imaging probe, which can achieve highly selective detection of endogenous and

exogenous $ONOO^-$ in living cells with excellent anti-interference capability, thereby providing a powerful tool for the visual monitoring of $ONOO^-$ in biological systems.

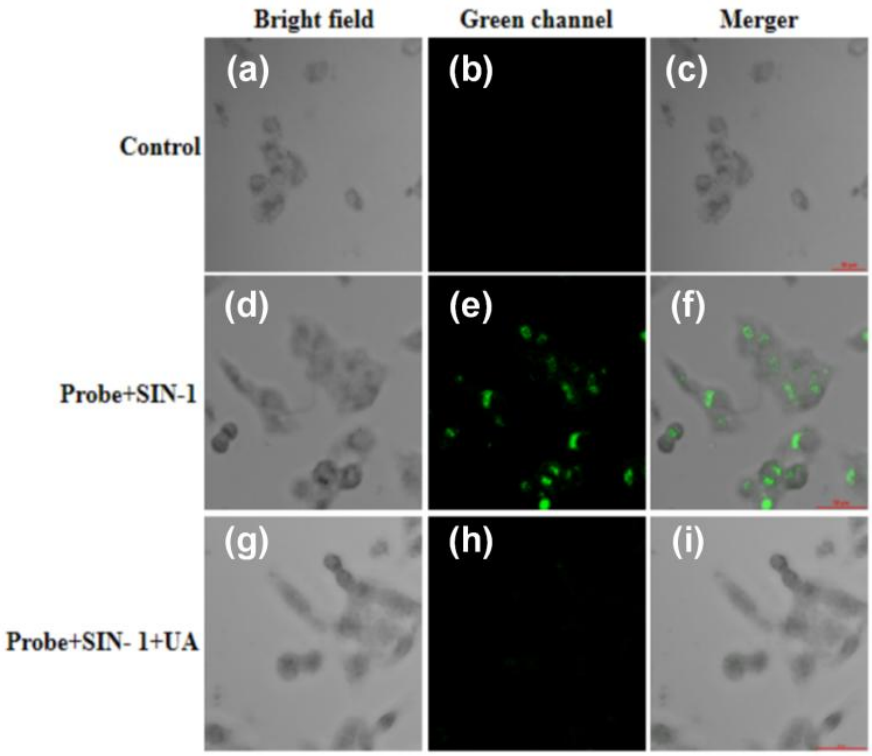


Figure 7. Fluorescence imaging of **M5** (2.0 μM) with exogenous $ONOO^-$ in HeLa cells. (a–c) Images of the cells in the absence of any treatment. (d–f) Images of the cells prestimulated with SIN-1 (100.0 μM) for 30.0 min. (g–i) Images of the cells prestimulated with SIN-1 (100.0 μM) for 30.0 min and UA (200.0 μM) for 10.0 min. Green channel: Ex = 405 nm, Em = 520–580 nm.

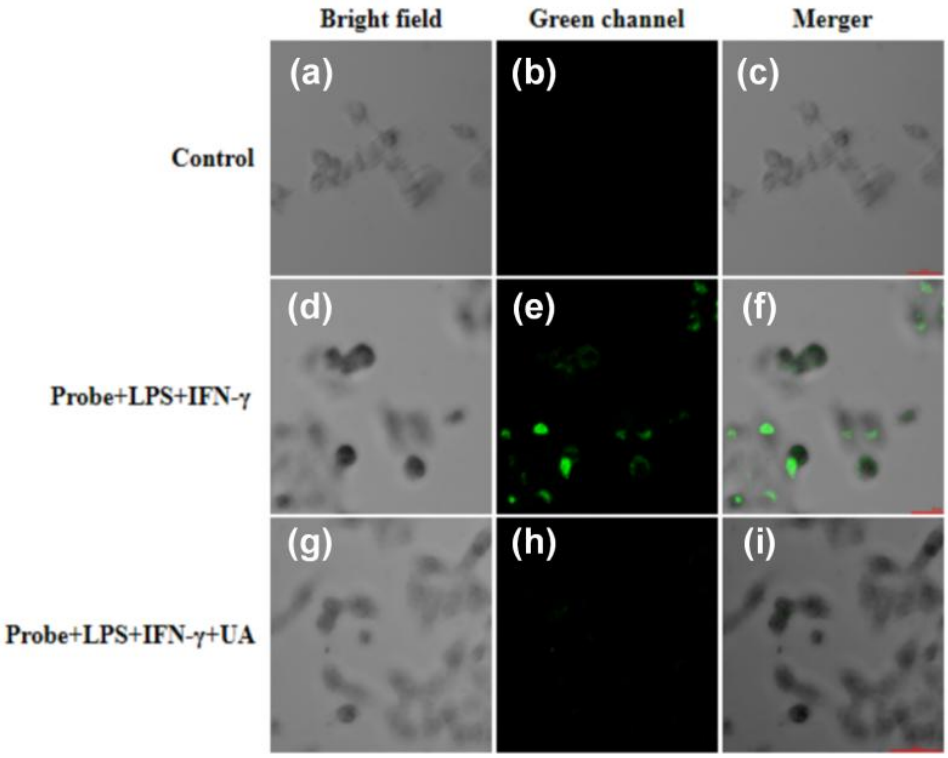


Figure 8. Fluorescence imaging of **M5** (2.0 μM) with endogenous $ONOO^-$ in HeLa cells. (a–c) Images of the cells in the absence of any treatment. (d–f) Images of the cells prestimulated with LPS (100 μg/mL) and IFN-γ (50 ng/mL) for 12 h. (g–i) Images of the cells prestimulated with LPS (100 μg/mL) and IFN-γ (50 ng/mL) for 12 h and UA (200.0 μM) for 10.0 min. Green channel: Ex = 405 nm, Em = 520–580 nm.

4. Conclusion

In summary, this study successfully developed a novel fluorescent probe **M5** based on a sulfonated quinoline–malononitrile–phenothiazine hybrid system, which enables the specific recognition and detection of $ONOO^-$. Relying on its typical D–π–A structural features, **M5** possesses excellent selectivity for $ONOO^-$ and favorable photostability. Meanwhile, this probe exhibits competitive analytical performance, including strong anti-interference capability against various common interfering species and a low detection limit of 0.30 μM. As summarized in Table S1, comparison with

representative $ONOO^-$ fluorescent probes reported in recent years further highlights the competitive fluorescence enhancement (52-fold) and relatively broad linear response range of **M5**. In addition, the probe has been successfully applied to fluorescence imaging of endogenous and exogenous $ONOO^-$ in living cells. These properties demonstrate that **M5** is a promising fluorescence "turn-on" probe, providing a useful tool for $ONOO^-$ detection and imaging in biological systems.

Acknowledgments

This work was supported by the Shandong Provincial Natural Science Foundation (ZR2024MB099, ZR2025QC136) and the Youth Science and Technology Innovation Support Program for Higher Education Institutions of Shandong Province (2024KJG054).

Declaration of competing interest

The authors declare that they have no conflicts of interest in this work.

Appendix A. Supplementary data

Electronic supplementary information (ESI) available: details of the experimental section, NMR data of products and intermediates, Figure S1–S19 and Table S1. Supplementary data to this article can be found online at https://doi. xxx.

Reference

[1] Pacher, P., Beckman, J. S., & Liaudet, L. (2007). Nitric oxide and peroxynitrite in health and disease. *Physiological Reviews*, 87, 315–424. https://doi.org/10.1152/physrev.00029.2006

[2] Zhang, J. J., Zhen, X., Zeng, J. F., & Pu, K. Y. (2018). A dual-modal molecular probe for near-infrared fluorescence and photoacoustic imaging of peroxynitrite. *Analytical Chemistry*, 90(15), 9301–9307. https://doi.org/10.1021/acs.analchem.8b01879

[3] Deng, Y., Shi, X., Hu, X. Y., Xu, L. L., Liu, X. Y., Gao, G., Wang, R., & Liang, G. L. (2023). A chemiluminescent probe for imaging peroxynitrite in inflammatory cells and tissues. *Analytical Chemistry*, 95(16), 6496–6500. https://doi.org/10.1021/acs.analchem.3c01124

[4] Kooy, N. W., Lewis, S. J., Royall, J. A., Ye, Y. Z., Kelly, D. R., & Beckman, J. S. (1997). Extensive tyrosine nitration in human myocardial inflammation: Evidence for the presence of peroxynitrite. *Critical Care Medicine*, 25(5), 812–819. https://doi.org/10.1097/00003246-199705000-00017

[5] Przedborski, S., Chen, Q., Vila, M., Giasson, B. I., Djaldatti, R., Vukosavic, S., Souza, J. M., Jackson-Lewis, V., Lee, V. M., & Ischiropoulos, H. (2001). Oxidative post-translational modifications of alpha-synuclein in the 1-methyl-4-phenyl-1,2,3,6-tetrahydropyridine (MPTP) mouse model of Parkinson's disease. *Journal of Neurochemistry*, 76(2), 637–640. https://doi.org/10.1046/j.1471-4159.2001.00174.x

[6] Smith, M. A., Richey Harris, P. L., Sayre, L. M., Beckman, J. S., & Perry, G. (1997). Widespread peroxynitrite-mediated damage in Alzheimer's disease. *Journal of Neuroscience*, 17(8), 2653–2657. https://doi.org/10.1523/JNEUROSCI.17-08-02653.1997

[7] Cao, J., An, W. W., Reeves, A. G., & Lippert, A. R. (2018). A chemiluminescent probe for cellular peroxynitrite using a self-immolative oxidative decarbonylation reaction. *Chemical Science*, 9(9), 2552–2558. https://doi.org/10.1039/C7SC05087A

[8] Wang, B., Ji, X., Ren, J., Ni, R., & Wang, L. (2017). Enhanced electrocatalytic activity of graphene-gold nanoparticles hybrids for peroxynitrite electrochemical detection on hemin-based electrode. *Bioelectrochemistry*, 118, 75–82

[9] Chen, Y. R., Chen, C. L., Chen, W., Zweier, J. L., Augusto, O., Radi, R., & Mason, R. P. (2004). Formation of protein tyrosine ortho-semiquinone radical and nitrotyrosine from cytochrome c-derived tyrosyl radical. *Journal of Biological Chemistry*, 279, 18054–18062

[10] Daiber, A., Oelze, M., August, M., Wendt, M., Sydow, K., Wieboldt, H., Kleschyov, A. L., & Munzel, T. (2004). Detection of superoxide and peroxynitrite in model systems and mitochondria by the luminol analogue L-012. *Free Radic. Res.*, 38, 259–269

[11] Zhang, W., Ma, M., Zhao, C., Dong, W., Ma, P., Song, D., & Sun, Y. (2025). Differentiated imaging of Hashimoto's thyroiditis against thyroid carcinoma by endogenous peroxynitrite activated near-infrared fluorescent probe. *Sensors and*

Actuators B: Chemical, 443, 138268. https://doi.org/10.1016/j.snb.2025.138268

[12] Yang, K., Liu, Y., Deng, M., Wang, P., Cheng, D., Li, S., & He, L. (2024). Imaging peroxynitrite in endoplasmic reticulum stress and acute lung injury with a near-infrared fluorescent probe. *Analytica Chimica Acta*, 1286, 342050. https://doi.org/10.1016/j.aca.2023.342050

[13] Zhang, C.-L., Zhang, Y., Zhang, Y. P., Guo, J.-H., Zhang, L., Liu, C., & Nie, S.-R. (2024). A novel fluorescent probe based on phenothiazine for recognition of Ni^{2+} and ClO^- and its applications. *Inorganic Chemistry Communications*, 162, 112079. https://doi.org/10.1016/j.inoche.2024.112079

[14] Liu, Q., Li, X., Xiao, M., Ai, Y., Liu, G., Ding, H., & Pu, S. (2023). A "Turn-on" fluorescent probe based on phenothiazine for selectively recognizing ClO^- and its practical applications. *Journal of Fluorescence*, 33, 2451–2459. https://doi.org/10.1007/s10895-023-03215-1

[15] Wang, X.-H., Sun, H.-J., Wang, Z.-H., Luan, J.-Y., Xin, S., Wang, K.-P., Fang, Y., & Hu, Z.-Q. (2026). Molecular engineering of a D–π–A–π–D scaffold for two-photon near-infrared imaging of peroxynitrite in vivo. *Dyes and Pigments*, 250, 113669. https://doi.org/10.1016/j.dyepig.2026.113669

[16] Lu, W., Yang, B., Guo, Z., Tian, Z., He, W., & Yang, T. (2024). Machine learning-based fluorescence sensor array: Accurate discrimination, quantitative assay of phenothiazine drugs via versatile DNA probes. *Sensors and Actuators B: Chemical*, 405, 135330. https://doi.org/10.1016/j.snb.2024.135330

[17] Shao, A. D., Guo, Z. Q., Zhu, S. J., Zhu, S. Q., Shi, P., Tian, H., & Zhu, W. H. (2014). Insight into aggregation-induced emission characteristics of red-emissive quinoline-malononitrile by cell tracking and real-time trypsin detection. *Chemical Science*, 5, 1383–1389. https://doi.org/10.1039/C3SC52783B

[18] Khan, F., & Misra, R. (2023). Recent advances in the development of phenothiazine and its fluorescent derivatives for optoelectronic applications. *Journal of Materials Chemistry C*, 11, 2786–2825. https://doi.org/10.1039/D2TC04326B

[19] Athira, P., Kappumchalil, R. N., Sachin, A. R., Yoosuf, M., Thomas, R., & Gopakumar, G. (2024). Intramolecular charge transfer and stimuli-responsive emission in cholesterol-appended phenothiazine–cyanostyryl-based donor–acceptor systems. *The Journal of Physical Chemistry A*, 128(20), 3935–3946. https://doi.org/10.1021/acs.jpca.4c00373

[20] Slodek, A., Zych, D., Zimosz, S., Szafraniec-Gorol, G., Kotowicz, S., Kubis, M., Kowalska-Szojda, K., Malarz, K., & Musioł, R. (2026). Spectroscopic and theoretical analysis of N-ethylphenothiazine derivatives: Alkyl chain length effects on solvatochromism, fluorescence efficiency, and excited-state polarity. *The Journal of Physical Chemistry B*, 130(10), 2843–2858. https://doi.org/10.1021/acs.jpcb.5c08011

[21] Yang, F., Song, X., Zhang, M., Ma, H., Zhang, S., Wang, W., Wang, R., Wang, Z., Yuan, Z., Ren, D., & Sun, W. (2024). Mitochondria-targeting phenothiazine-based ratiometric fluorescent probe for visual and rapid detection of hypochlorous acid in living cells and zebrafish. *Dyes and Pigments*, 229,

112258. https://doi.org/10.1016/j.dyepig.2024.112258
[22] Chen, M., Chen, X., Wang, Y., Fan, X., Chen, T., & Liang, Z. (2022). An ESIPT fluorescent probe for ultrarapid HClO detection during reagent-stimulated oxidative stress in cells and zebrafish. *Sensors and Actuators B: Chemical*, 371, 132545. https://doi.org/10.1016/j.snb.2022.132545
[23] Huang, T., Yan, S., Yu, Y., Xue, Y., Yu, Y., & Han, C. (2022). Dual-responsive ratiometric fluorescent probe for hypochlorite and peroxynitrite detection and imaging in vitro and in vivo. *Analytical Chemistry*, 94(2), 1415–1424. https://doi.org/10.1021/acs.analchem.1c04729
[24] He, L., Liu, H., Wu, J., Cheng, Z., & Yu, F. (2022). Construction of a mitochondria–endoplasmic reticulum dual-targeted red-emitting fluorescent probe for imaging peroxynitrite in living cells and zebrafish. *Chemistry – An Asian Journal*, 17(14), e202200388. https://doi.org/10.1002/asia.202200388
[25] Yan, H., Xu, X., Li, J., Xie, P., Cao, W., Yang, X., & Ye, Y. (2023). A novel fluorescence-on fluorescent probe for $ONOO^-$ detection in HeLa cells. *Journal of Photochemistry and Photobiology A: Chemistry*, 440, 114638. https://doi.org/10.1016/j.jphotochem.2023.114638
[26] Liu, F., Li, M., Li, W., Ren, Y., Zhang, M., Zhang, H., Wang, P., Wu, Y., Wang, K., Wang, X., Chen, X., & Tang, J. (2024). Peroxynitrite-activated fluorescent probe with two reaction triggers for pathological diagnosis and therapeutic evaluation of inflammation. *Bioorganic Chemistry*, 147, 107362. https://doi.org/10.1016/j.bioorg.2024.107362
[27] Huang, Y., Zhang, Y., Gong, Z., Tan, Z., Ding, H., Ji, Y., Fan, C., Liu, G., & Pu, S. (2026). AIE functionality ratiometric fluorescent probe based on quinoline-malononitrile for detection of $ONOO^-$ and its application in bioimaging. *Spectrochimica Acta Part A: Molecular and Biomolecular Spectroscopy*, 346, 126855. https://doi.org/10.1016/j.saa.2025.126855
[28] Yu, D.-H., Wang, J.-Q., Kong, L., & Liu, Z.-D. (2011). 10-Ethyl-10H-phenothiazine-3-carbaldehyde. *Acta Crystallographica Section E: Structure Reports Online*, 67(12), o3344. https://doi.org/10.1107/S1600536811047799
[29] Geng, L., Xu, W., Xia, Q., Zhao, J., Jia, C., Yang, M., Chen, P., Cheng, Y., He, L., Xu, Z., Chen, H., Zhang, Y., Gong, S., & Liu, R. (2018). A far-red-emissive AIE active fluorescent probe with large stokes shift for detection of inflammatory bowel disease in vivo. *Journal of Materials Chemistry B*, 6, 809–815. https://doi.org/10.1039/c7tb03168h
[30] Xu, M., Li, R., Li, X., Lv, G., Li, S., Sun, A., Zhou, Y., & Yi, T. (2019). NIR fluorescent probes with good water-solubility for detection of amyloid beta aggregates in Alzheimer's disease. *Journal of Materials Chemistry B*, 7, 5535–5540. https://doi.org/10.1039/c9tb01012b
[31] Huang, W., Du, X., Zhang, C., Zhang, S., Zhang, J., & Yang, X.-F. (2022). Rational design of a dual-channel fluorescent probe for the simultaneous imaging of hypochlorous acid and peroxynitrite in living organisms. *Analytical Chemistry*, 94(50), 17485–17493. https://doi.org/10.1021/acs.analchem.2c03661

[32] Zhang, W., Song, W., & Lin, W. (2021). A novel ER-targeted two-photon fluorescent probe for monitoring abnormal concentrations of HClO in diabetic mice. *Journal of Materials Chemistry* B, 9, 7381–7385. https://doi.org/10.1039/D1TB01327K

[33] Li, M. Y., Li, K., Liu, Y. H., Zhang, H., Yu, K. K., Liu, X., & Yu, X. Q. (2020). Mitochondria-immobilized fluorescent probe for the detection of hypochlorite in living cells, tissues, and zebrafishes. *Analytical Chemistry*, 92, 3262–3269. https://doi.org/10.1021/acs.analchem.9b05102

[34] Fang, H., Chen, Y., Geng, S., Yao, S., Guo, Z., & He, W. (2022). Super-resolution imaging of mitochondrial HClO during cell ferroptosis using a near-infrared fluorescent probe. *Analytical Chemistry*, 94, 17904–17912. https://doi.org/10.1021/acs.analchem.2c03887

[35] Winterbourn, C. C. (2008). Reconciling the chemistry and biology of reactive oxygen species. *Nature Chemical Biology*, 4, 278–286. https://doi.org/10.1038/nchembio.85

[36] Pattison, D. I., & Davies, M. J. (2006). Evidence for rapid inter- and intramolecular chlorine transfer reactions of histamine and carnosine chloramines: implications for the prevention of hypochlorous-acid-mediated damage. *Biochemistry*, 45, 8152–8162. https://doi.org/10.1021/bi060348s

[37] Fang, J., Li, X., Gao, C., Gao, S., Li, W., Seidu, M. A., & Zhou, H. (2024). A unique phenothiazine-based fluorescent probe using benzothiazolium as a reactivity regulator for the specific detection of hypochlorite in drinking water and living organisms. *Talanta*, 268, 125299. https://doi.org/10.1016/j.talanta.2023.125299

[38] Fang, Y., Chen, R., Qin, H., Wang, J., Zhang, Q., Chen, S., Wen, Y., Wang, K., & Hu, Z. (2021). A chromene based fluorescence probe: Accurate detection of peroxynitrite in mitochondria, not elsewhere. *Sensors and Actuators B: Chemical*, 334, 129603. https://doi.org/10.1016/j.snb.2021.129603

[39] Wu, L., Liu, J., Tian, X., Groleau, R. R., Bull, S. D., Li, P., Tang, B., & James, T. D. (2021). Fluorescent probe for the imaging of superoxide and peroxynitrite during drug-induced liver injury. *Chemical Science*, 12, 3921–3928. https://doi.org/10.1039/D0SC05937D

[40] Wu, Q., Hu, Z., Zhang, G., Jin, Y., & Wang, Z. (2024). BODIPY-based ratiometric fluorescent probe for sensing peroxynitrite in inflammatory cells and tissues. *Biosensors*, 14(12), 638. https://doi.org/10.3390/bios14120638

[41] Chen, X., Wang, Y., Zhao, X.-L., Fan, Y.-C., Bie, H.-Y., Wu, W.-N., & Xu, Z.-H. (2024). Construction of a dual-excitation ratiometric fluorescent probe for determining peroxynitrite levels in living cells and zebrafish. *Spectrochimica Acta Part A: Molecular and Biomolecular Spectroscopy*, 313, 124084. https://doi.org/10.1016/j.saa.2024.124084

[42] Tang, J., Deng, S., Xie, Y., Li, S., Qiao, Y., Zhu, L., Guo, J., Zhou, J., & Ye, Y. (2024). Visualizing HClO and $ONOO^-$ fluxes based on bifunctional fluorescent probe. *Dyes and Pigments*, 227, 112183. https://doi.org/10.1016/j.dyepig.2024.112183

[43] Shang, J., Yang, Y., Sun, Y., Gao, W., Ma, K., Wang, C., Yu, X., Li, L., Zheng, J., Zhao, N., Shu, X., & Zhang, Y. (2025). Real-time monitoring of $ONOO^-$ in cerebral ischemia-reperfusion injury mouse models using a hydrazine-based NIR fluorescent probe. *Redox Biology*, 80, 103494. https://doi.org/10.1016/j.redox.2025.103494

[44] Wang, H., Tang, B., Xiu, T., Zhang, X., Zhu, L., Bi, H., & Li, P. (2025). A sequentially activated probe for simultaneous fluorescence imaging of $ONOO^-$ and HOBr in brain to indicate Alzheimer's Disease. *Sensors and Actuators B: Chemical*, 440, 137947. https://doi.org/10.1016/j.snb.2025.137947

[45] Liu, J., Zhao, X., Zhang, L., Zhou, H., Li, X., Zheng, G., Zhou, X., Peng, Y., & Zhang, J. (2026). A FRET-based ratiometric fluorescent chemosensor for mitochondrial $ONOO^-$ detection with application to rheumatoid arthritis. *Sensors and Actuators B: Chemical*, 451, 139326. https://doi.org/10.1016/j.snb.2025.139326

Springer Nature or its licensor (e.g. a society or other partner) holds exclusive rights to this article under a publishing agreement with the author(s) or other rightsholder(s); author self-archiving of the accepted manuscript version of this article is solely governed by the terms of such publishing agreement and applicable law.

Supplementary Files

This is a list of supplementary files associated with this preprint. Click to download.

- Supplementarymaterial1021.docx